

# Morphology and chemical composition of cobalt germanide islands on Ge(001): in-situ nanoscale insights into contact formation for Ge-based device technology

M Ewert<sup>1</sup>, Th Schmidt<sup>1</sup>, J I Flege<sup>1</sup>, I Heidmann<sup>1</sup>, T Grzela<sup>2</sup>,  
W M Klesse<sup>2</sup>, M Foerster<sup>3</sup>, L Aballe<sup>3</sup>, T Schroeder<sup>2,4</sup>, and J Falta<sup>1</sup>

<sup>1</sup> Institute of Solid State Physics, University of Bremen, Otto-Hahn-Allee 1, 28359 Bremen, Germany

<sup>2</sup> IHP, Im Technologiepark 25, 15236 Frankfurt (Oder), Germany

<sup>3</sup> ALBA Synchrotron Light Facility, Carretera BP 1413, km 3.3, Cerdanyola del Vallès, Barcelona 08290, Spain

<sup>4</sup> BTU Cottbus-Senftenberg, Institute of Physics and Chemistry, Konrad-Zuse-Str. 1, 03046 Cottbus, Germany

E-mail: tschmidt@ifp.uni-bremen.de

Date: September 19, 2018

**Abstract.** The reactive growth of cobalt germanide on Ge(001) was investigated by means of *in-situ* x-ray absorption spectroscopy photoemission electron microscopy (XAS-PEEM), micro-illumination low-energy electron diffraction ( $\mu$ -LEED), and *ex-situ* atomic force microscopy (AFM). At a Co deposition temperature of 670°C, a rich morphology with different island shapes and dimensions is observed, and a correlation between island morphology and stoichiometry is found. Combining XAS-PEEM and  $\mu$ -LEED, we were able to identify a large part of the islands to consist of CoGe<sub>2</sub>, with many of them having an unusual epitaxial relationship: CoGe<sub>2</sub>[ $\bar{1}10$ ](111) || Ge[ $\bar{1}10$ ](001). Side facets with (112) and (113) orientation have been found for such islands. However, two additional phases were observed, most likely Co<sub>5</sub>Ge<sub>7</sub> and CoGe. The occurrence of these intermediate phases is promoted by defects, as revealed by comparing growth on Ge(001) single crystals and on Ge(001)/Si(001) epilayer substrates.

PACS numbers: 61.46.Hk, 68.55.-a, 61.05.cj, 61.05.jh, 68.37.Nq, 68.37.Ps

Submitted to: *Nanotechnology*

**Keywords:** cobalt germanide, stoichiometry, facets, epitaxial relationship, LEEM, XAS-PEEM, AFM

## 1. Introduction

In state-of-the-art silicon based complementary metal oxide semiconductor (CMOS) electronics, the integration of germanium becomes more and more important, since it provides materials properties superior to Si. In addition to an increased performance resulting from a higher charge carrier mobility [1], the Ge band structure can be engineered to exhibit a quasi-direct bandgap, enabling the fabrication of laser structures [2–6]. Especially for such high-current applications, one of the challenges with this materials approach is to prepare stable, low-resistance contacts that are compatible with current processing technologies. In this respect, a high control over morphology and chemical composition is required, since inhomogeneous Schottky barriers limit the overall device performance [7].

Based on the experience with nickel and cobalt silicides as contacts for Si devices, nickel and cobalt germanides are considered promising for fabrication of high-quality contacts on Ge. In the following, we address the growth of cobalt germanides on Ge(001). In comparison to the Ni–Ge system [8], the Co–Ge system exhibits a more complex bulk phase diagram. As a consequence, it is important to determine and to control which phase is formed under which growth conditions.

The most common scheme to produce cobalt germanides on germanium is to deposit Co which then reacts with the Ge from the substrate. In general, two growth techniques are distinguished in this context: (i) solid-phase epitaxy (SPE), i.e., Co deposition at room temperature and subsequent annealing and (ii) reactive growth by Co deposition at elevated temperature. In the present work we focus on the less-studied reactive growth. As in the case of cobalt silicide [9, 10] by far not all bulk phases [11] are observed in epitaxial cobalt germanide structures. Nevertheless, both for reactive growth and SPE of cobalt germanides, at least three different phases have been observed [12, 13]: CoGe, Co<sub>5</sub>Ge<sub>7</sub>, and CoGe<sub>2</sub>. For Ge-rich conditions, such as in case of small Co deposits on a Ge substrate, a CoGe<sub>2</sub> stoichiometry is expected from the bulk phase diagram [11]. This is beneficial, since CoGe<sub>2</sub> has a low ohmic resistance. Moreover, with the epitaxial relationship CoGe<sub>2</sub>[100](001) || Ge[100](001), growth with very little lattice mismatch (about 0.3 %) is possible. This epitaxial relationship has been proposed earlier [14], and has experimentally been observed by Choi *et al.* with scanning tunneling microscopy (STM), who find two different types of surface termination of the germanide, both

with a  $(\sqrt{2} \times \sqrt{2})R45^\circ$  surface reconstruction [15]. Despite similar growth conditions and similar island morphologies, different surface periodicities have been reported in other STM studies [16, 17]. Such an occurrence of different surface structures may be related to different, simultaneously occurring epitaxial relationships. The latter have been demonstrated both for Co<sub>5</sub>Ge<sub>7</sub> and for CoGe<sub>2</sub>, by transmission electron microscopy [18] and, in particular, by x-ray diffraction (XRD) [19].

For SPE, Goldfarb and Briggs propose a phase sequence [13] that does not lead directly to CoGe<sub>2</sub>. Instead, at lower annealing temperatures, they propose the formation of Co<sub>5</sub>Ge<sub>7</sub> and possibly still further intermediate phases such as Co<sub>2</sub>Ge and CoGe. This is in agreement, for instance, with earlier XRD experiments [12] by Ashburn *et al.* Under SPE conditions, these authors find a complete transition from Co<sub>5</sub>Ge<sub>7</sub> to CoGe<sub>2</sub> for rapid annealing at 600°C. In a more recent study [19], an even higher transition temperature of 680°C was found. Contrary, the direct formation of virtually pure CoGe<sub>2</sub> has been reported for temperatures as low as 500°C in case of reactive growth [13].

In recent STM studies [16, 17], two different types of cobalt germanide islands were observed for SPE with moderate annealing temperatures up to 500°C: (a) islands with a rectangular outline and a flat top facet, i.e., with a trapezoidal cross section, and (b) elongated, narrow islands with a peaked cross section. The latter island type has been reported to be preferred for large island sizes [16] and for higher temperatures [17].

Despite the fact that the presence of different types of islands might point to different stoichiometries, hardly any of the numerous studies on cobalt germanide growth on Ge(001) provides a link between island shape and stoichiometry. In the present work we aim at bridging this gap and focus on the question whether island morphology and chemical composition of cobalt germanide islands on Ge(001) are correlated, and, in addition, whether high-temperature growth is a viable approach to produce single-phase CoGe<sub>2</sub>. For this purpose, we have chosen an experimental *in-situ* approach that allows to obtain real-space, reciprocal-space and spectroscopic information from the very same structures on a local scale, i.e., we used low-energy electron microscopy (LEEM), micro-illumination low-energy electron diffraction ( $\mu$ -LEED), and photoemission electron microscopy combined with x-ray absorption spectroscopy (XAS-PEEM) in order to simultaneously investigate the morphology of the cobalt germanide structures and probe their chemical composition

with a spatial resolution of a few tens of nanometers.

## 2. Experimental

The XAS-PEEM and  $\mu$ -LEED experiments presented in the following were performed *in situ* at the XPEEM experimental station of the CIRCE beamline [20] at the ALBA Synchrotron Light Facility (Spain).

Two types of substrates were used in this study: On the one hand, single-crystalline Ge(001) samples cut from Sb-doped wafers were used, and, on the other hand, 5  $\mu\text{m}$  thick Ge template layers epitaxially grown on Si(001), a less perfect substrate type but technologically more relevant. The latter were prepared at IHP, Frankfurt (Oder), Germany, using an approach published elsewhere [21]. The substrates were cleaned by three cycles of  $\text{Ar}^+$  ion sputtering followed by annealing at 800  $^\circ\text{C}$  for 30 min. The samples were heated by electron bombardment from the backside, and the temperature was monitored by a thermocouple attached closely to the sample and cross-calibrated by an infrared pyrometer and, using  $\mu$ -LEED, by the Ge(001) ( $2\times 1$ ) to ( $1\times 1$ ) phase transition temperature [22] at 680  $^\circ\text{C}$ .

Cobalt germanide was grown slightly below this transition temperature, at about 670  $^\circ\text{C}$ . For this purpose, cobalt was evaporated at a deposition rate of 0.34  $\text{\AA}$  per minute from an electron beam evaporator containing a Co rod of 99.99 % purity, with typical deposits of about 20  $\text{\AA}$ .

After growth, the surface was investigated by LEEM,  $\mu$ -LEED [23] and XAS-PEEM [24, 25]. For the latter, the samples were illuminated with a monochromatic, focused x-ray beam. The photon energy was scanned across the Co L absorption edge. Secondary electrons with a very low kinetic energy (typically 0.5 eV), which provide a measure for the local x-ray absorption, were used for imaging.

*In-situ*  $\mu$ -LEED images were recorded using a 500 nm illumination aperture, in an electron energy range from 2 eV up to 100 eV. Since with LEEM and related techniques it is rather difficult to assess the height of nanostructures, complementary *ex-situ* atomic-force microscopy (AFM) investigations of the samples were conducted at IHP, Frankfurt(Oder), with a Bruker/Veeco Dimension 5000 instrument operated under ambient conditions in tapping mode, using an  $n^+$ -doped Si cantilever.

## 3. Results and Discussion

The XAS-PEEM image in Fig. 1 (a) illustrates the surface morphology after Co germanide growth at 670  $^\circ\text{C}$  on a Ge(001) template layer. Since the image was recorded with a photon energy slightly above the Co  $L_3$  edge, the contrast reflects the Co distribution on the surface: Co germanide islands appear bright, whereas the Ge substrate appears dark. Obviously, islands have formed with a broad variety in size and shape, whereas the remaining substrate area does not seem to contain any Co, which

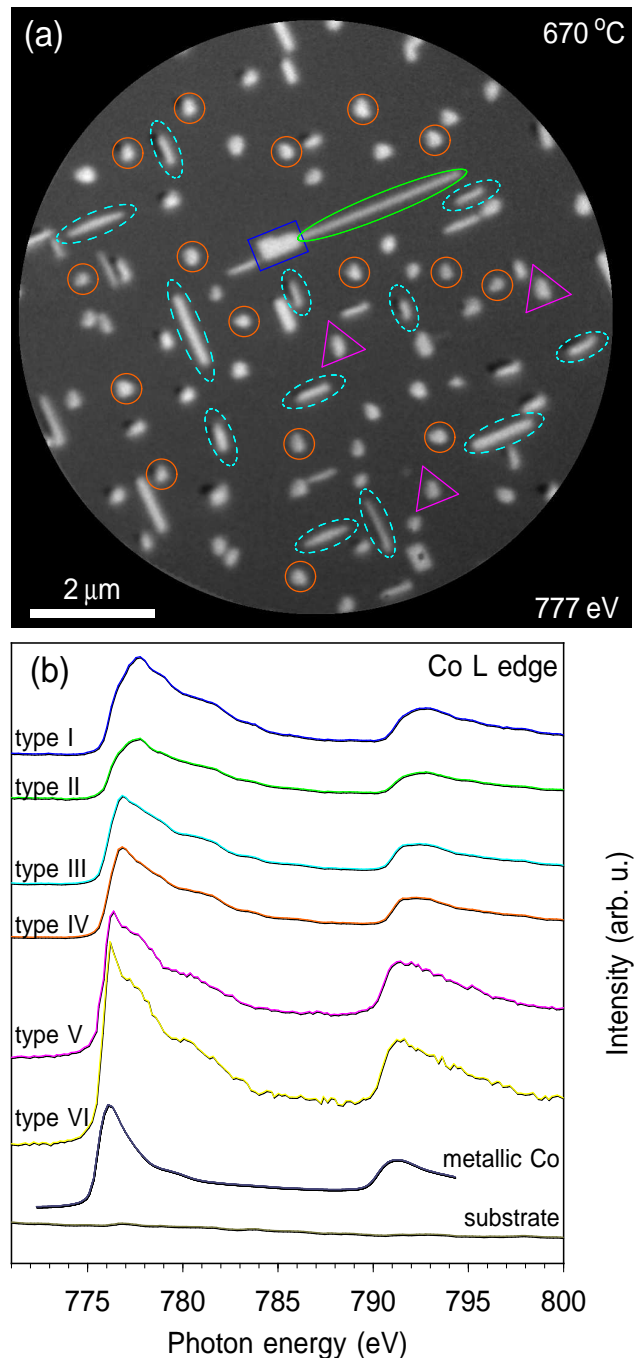


**Figure 1.** (a) XAS-PEEM image after Co deposition on a Ge(001) epilayer, showing islands of various types, marked with specific symbols (see text). (b) Local x-ray absorption spectra for type-I to type-VI islands, metallic cobalt, and for the region between islands (from top to bottom). The metallic spectrum has been taken from a Co layer deposited at RT (without annealing).

points to a Volmer-Weber growth mode. In Fig. 1, several islands have been marked, using equal symbols for islands with similar morphology. From the XAS-PEEM data, together with typical AFM data, such as shown in Fig. 2, different types of islands can be categorized: large and

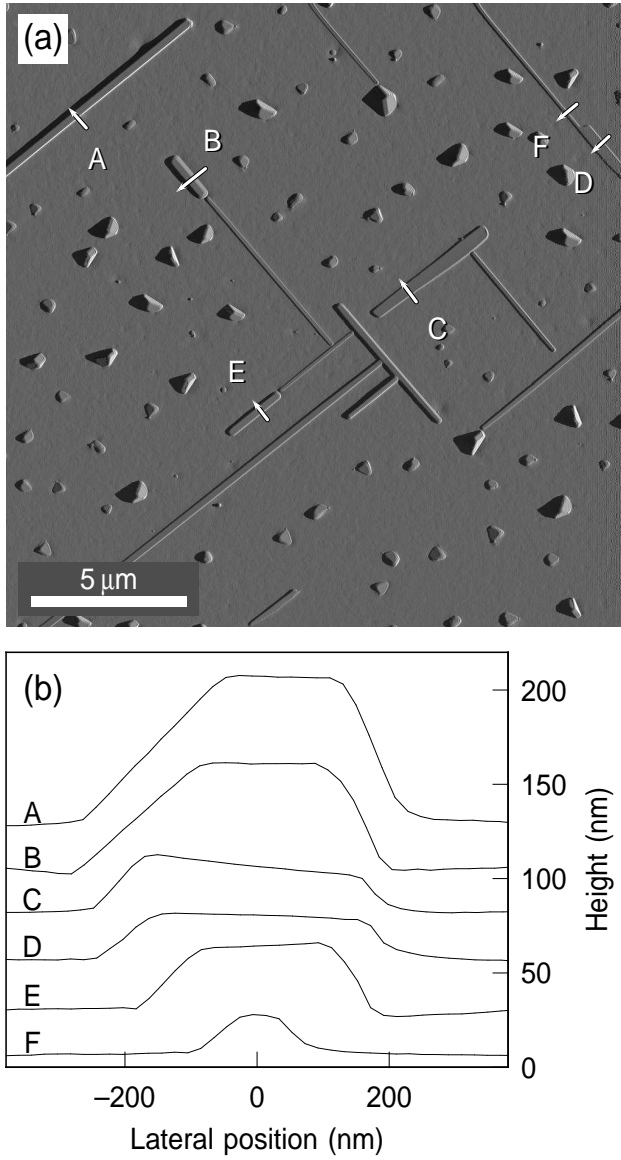


**Figure 2.** (a) AFM image after Co deposition on a Ge(001) single crystal and (b) several height profiles taken on different germanide islands as marked by white arrows and labels A–F in (a). Note that islands A–E are of type I, while F is a type-II islands. The compact islands on this surface are all of type V.

wide rectangular islands with a flat top facet (type I, blue rectangle in Fig. 1); narrow, very long islands without a flat top facet (type II, green ellipse), elongated narrow, but rather short and low islands without flat top facet (type III, dashed cyan ellipses); very compact and rather high islands (type IV, red circles); and small, irregularly shaped islands (type V, purple triangles). The anisotropic island types (type I to type III) are strictly aligned with the  $[110]$  or the  $[1\bar{1}0]$  substrate direction, i.e., they show a  $0^\circ$  or  $90^\circ$  azimuthal orientation. In very few cases, elongated islands are also found with  $45^\circ$  orientation (type VI, not present in Fig. 1). Typical dimensions of the different island types are

summarized in Tab. 1.

Interestingly, all six island types are observed for growth on Ge(001) template layer substrates, but only type-I, type-II, type-V, and type-VI islands are observed when using Ge(001) single-crystal substrates. Therefore, we conclude that the presence of type-III and type-IV islands on the Ge template layers is induced by defects.

Fig. 2 shows typical AFM data obtained from Co germanide islands grown on a single-crystal substrate. It can clearly be seen from Fig. 2 (a) that the compact islands have pronounced side facets. However, these type-V islands exhibit many different azimuthal orientations in contrast to the elongated islands.

The line profiles in Fig. 2 (b) show the presence of flat-top (profiles A–E) and peaked (profile F) islands. The top facets are, in general, not perfectly parallel to the substrate surface. In Fig. 2 (b), the largest tilt of about  $2.0^\circ$  occurs for the profile of the type-I island labeled “C”. The tilt observed here is not attributed to a misalignment of the instrument; a similar tilt angle has also been observed with LEED, as described below. It points to a small-angle grain boundary between Ge and the germanide.

Local Co L edge x-ray absorption spectra, extracted from XAS-PEEM image stacks, reveal the presence of Co in all island types, as shown in Fig. 1 (b). The regions between the islands, however, do not show a Co absorption signal (see bottom curve in Fig. 1 (b)). Hence, the regions between islands are virtually free of Co, indicative of a Volmer-Weber growth mode. Despite the similarity of the absorption spectra from the different island types, there are also significant differences. The spectra for type-V and type-VI islands show a sharp peak very close to the rising edge. In contrast, the spectra for type-I and type-II islands show a broader maximum that appears at higher photon energy. In this respect, the spectra of type-III and type-IV islands exhibit an intermediate shape and peak position. Hence, three different XAS fingerprints can be distinguished in Fig. 1 (b), pointing to the presence of three different Co germanide phases.

Before we continue with the interpretation of this spectroscopic result, we turn to an independent phase identification by means of  $\mu$ -LEED. For this purpose, a type-I island has been selected, since this island type is, on the hand, one of the most prominent ones, and, on the other hand, provides a flat top facet, which simplifies the analysis. The illuminated area in this experiment contained the center part of the type-I islands, one of its side facets, and, for reference, a small part of the substrate region next to the islands. Figure 3 (a) shows the averaged  $\mu$ -LEED pattern obtained over an energy range from 3 to 33 eV. Due to the constant final kinetic energy in the imaging column, the LEED spots from a flat surface do not move on the screen of a LEEM instrument, in contrast to conventional LEED optics [23]. Indeed, discrete LEED spots are visible in Figure 3 (a), which therefore can be attributed to the



**Table 1.** Typical morphologies of different island types as determined from LEEM, XAS-PEEM, and AFM.

	length ( $\mu\text{m}$ )	width (nm)	height (nm)	shape
type I	0.5 – 5	220 – 700	32 – 65	elongated, flat-top
type II	2.7 – 11.5	220 – 300	18 – 50	elongated, peaked
type III*	0.5 – 1.1	230 – 270	10 – 32	elongated, peaked
type IV*	$\sim 0.4$	$\sim 320$	42 – 65	compact
type V	$\sim 0.4$	$\sim 400$	32 – 45	compact, faceted
type VI**	$\sim 1.6$	$\sim 180$	$\sim 20$	elongated 45°

\* only on epilayer substrates

\*\* rare occurrence

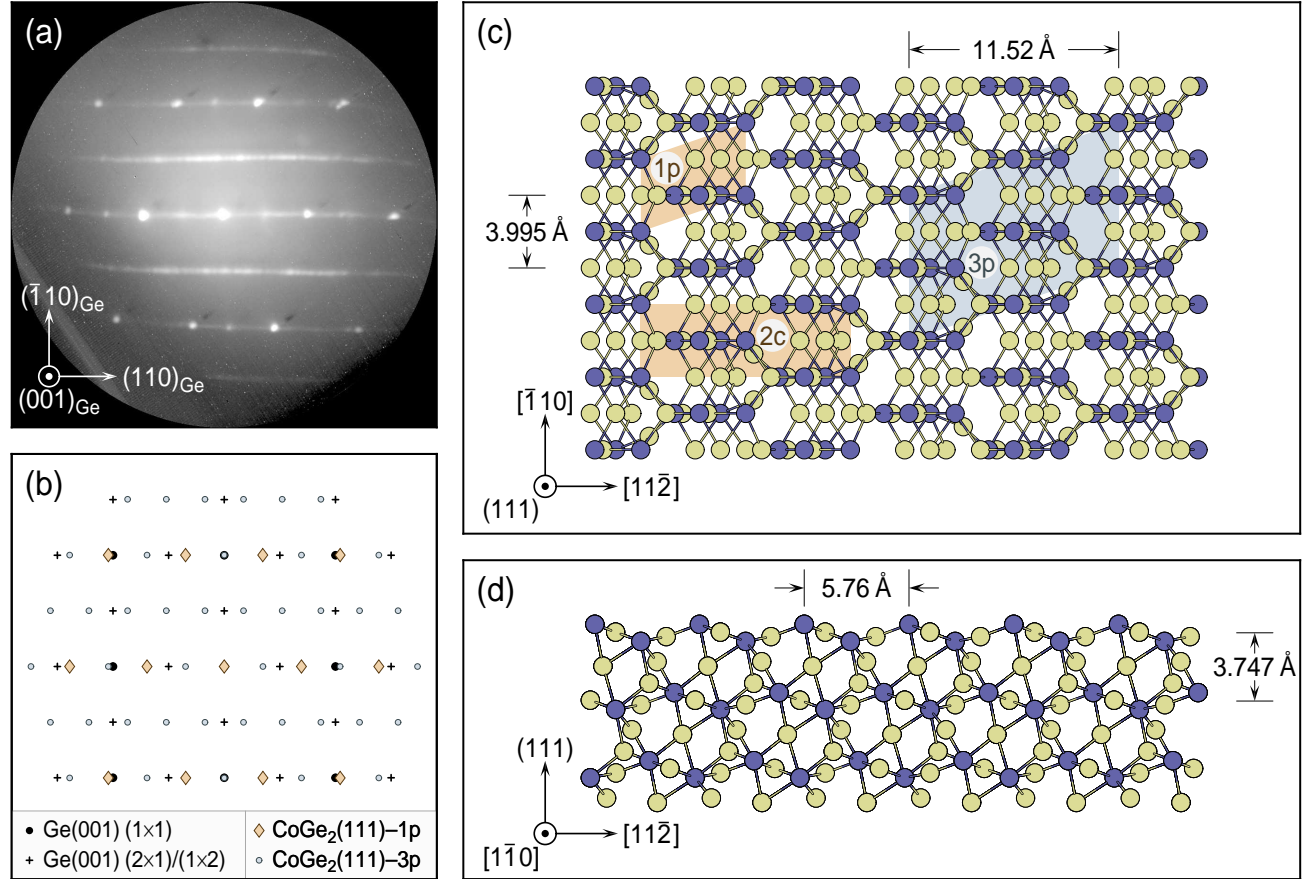


**Figure 3.** (a) Micro-LEED pattern taken on the edge of a type-I island grown on a Ge(001) epilayer, averaged over an electron energy range from 3 to 33 eV. (b) LEED spot positions expected for different unit meshes: large black dots (●) dots correspond to Ge(001)-(1×1); plus signs (+) mark superstructure spots from Ge(001)-(1×2) and (2×1); large reddish diamonds (◆) originate from the small oblique unit mesh labeled “1p” in the top view onto the Co-terminated CoGe<sub>2</sub>(111) surface in frame (c); small blue dots (○) mark the additional spots expected for the large oblique unit mesh labeled “3p” in (c). (c) Top view and (d) side view of the bulk-terminated CoGe<sub>2</sub>(111) surface according to the bulk structure reported in Ref. 26. Blue (dark) spheres correspond to Co, amber (bright) spheres to Ge atoms.

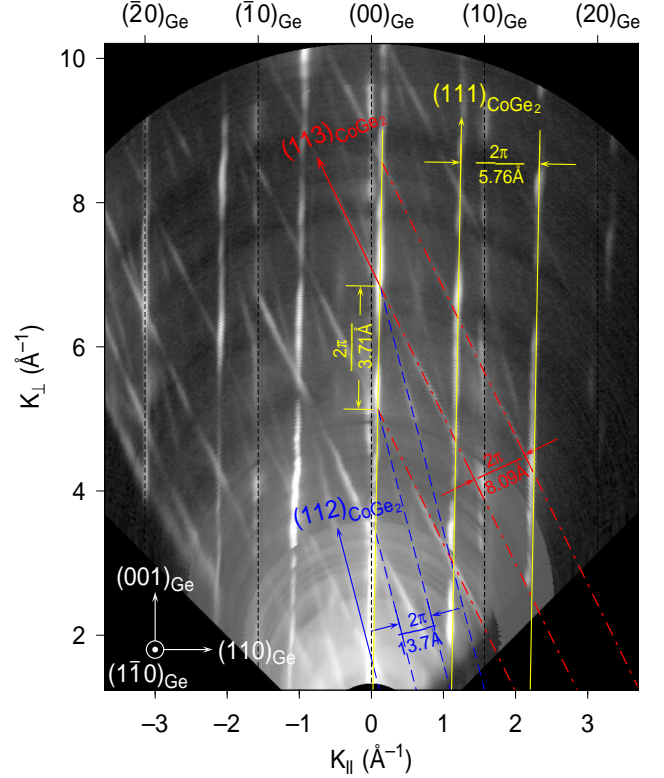
substrate and the top-facet of the type-I island. This discrete pattern is superimposed by streaks running from left to right in Fig. 3(a). These streaks in the energy-averaged image originate from LEED spots related to the island’s side facet(s), since spots from a tilted surface do move on the screen with electron energy. For clarity, we first analyze the discrete part of the LEED pattern, which is very similar to the sketch in Fig. 3(b).

From the Ge(001) substrate, a square-symmetry LEED pattern is expected as marked by black dots (integer spots) and plus-marks (superstructure spots from 2×1 reconstruction in two 90° rotational domains) in Fig. 3(b). Since the illuminated substrate area in the  $\mu$ -LEED experiment was very small, these spots are rather faint in the experimental LEED pattern shown in Fig. 3(a). The most intense spots correspond to the reddish diamonds in Fig. 3(b)

**Table 2.** Bulk unit cell parameters of Ge and some of its cobalt alloys.

	space group	$a$ (Å)	$b$ (Å)	$c$ (Å)	$\alpha$	$\beta$	$\gamma$	Ref.
Ge	227	5.658	5.658	5.658	90°	90°	90°	1
CoGe <sub>2</sub>	41	5.65	5.65	10.80	90°	90°	90°	26
		5.670	5.670	10.796	90°	90°	90°	27
Co <sub>5</sub> Ge <sub>7</sub>	107	7.626	7.626	5.802	90°	90°	90°	28
CoGe	12	11.65	3.807	4.945	90°	101.1°	90°	27
		11.63	3.801	4.935	90°	100.9°	90°	28

and have to be attributed to the top facet of the germanide island. They form an oblique pattern, typical of a centered rectangular unit mesh. Their spacing along the the bottom-up axis of the LEED pattern (Ge( $\bar{1}10$ ) direction) is the same as for the substrate spots, i.e., within the experimental resolution the germanide growth is pseudomorphic or lattice-matched with respect to the Ge substrate along its  $[\bar{1}10]$  direction. This is also the direction along which the germanide island is elongated; hence, a low lattice mismatch is energetically favorable in this direction. The best lattice match for low-index planes and directions for CoGe and Co<sub>5</sub>Ge<sub>7</sub> that comply with a rectangular LEED-pattern is obtained for (cf. Tab. 2) CoGe[010]  $\parallel$  Ge $[\bar{1}10]$ , and Co<sub>5</sub>Ge<sub>7</sub>[100]  $\parallel$  Ge $[\bar{1}10]$ , with a lattice mismatch of almost 5 % along the Ge $[\bar{1}10]$  direction in both cases. It seems very unlikely that such a large mismatch persists over such mesoscopic islands. In contrast, a lattice mismatch of less than 0.3 % occurs for CoGe<sub>2</sub> $[\bar{1}10]$  along Ge $[\bar{1}10]$  (cf. Tab. 2). In fact, the complete LEED pattern can be explained in terms of the CoGe<sub>2</sub> structure, as described in the following. We emphasize at this point that the previously proposed epitaxial relationship [13, 15] with CoGe<sub>2</sub>(001) parallel to Ge(001) can be excluded in this case, since this would require a LEED pattern with square symmetry. Instead, our data reveal the previously unreported CoGe<sub>2</sub> $[\bar{1}10](111) \parallel \text{Ge}[\bar{1}10](001)$  orientation shown in Fig. 3(c) and (d). Figure 3(c) is a top view of the CoGe<sub>2</sub>(111) surface, using the atomic positions within the bulk unit cell as determined by Schubert and Pfisterer [26]. The primitive surface unit mesh is the large blue parallelogram marked “3p” in Fig. 3(c). When only the two uppermost atomic layers are considered, however, the primitive surface unit mesh is given by the small parallelogram marked “1p”; alternatively, the non-primitive, centered rectangular unit mesh marked “2c” can be used. Even when more than two layers are considered, only few atoms violate the surface periodicity defined by “1p” (or, equivalently, “2c”). Therefore, the most intense spots of the LEED pattern will correspond to this reciprocal unit cell (marked by diamonds in Fig. 3(b)). The small deviations, leading to the actually larger “3c” unit mesh, produce additional spots which are expected to be relatively weak (marked by blue

**Figure 4.** Reciprocal-space map in the Ge ( $\bar{1}10$ )-(001) plane, taken at the edge of a type-I island.

dots in Fig. 3(b)). This model agrees very well with the experimental LEED pattern in Fig. 3(a).

Figure 4 shows a reciprocal-space map in the Ge(001)-( $\bar{1}10$ ) plane, extracted from a series of  $\mu$ -LEED images taken as a function of electron energy [29, 30]. Reciprocal-lattice rods with a periodicity of  $2\pi/4.00 \text{ \AA}$  run along the vertical direction, i.e., along the Ge(001) direction. They are identified as integer reciprocal-lattice rods of the Ge(001) substrate and marked by dashed black lines. The half-order rods generated by the  $2 \times 1$  surface reconstruction are hardly visibly. (Best to be seen is the  $(\frac{1}{2}0)$  rod.) The most intense rods (solid yellow lines) are attributed to the top facet of the type-I island. These rods are not perfectly aligned along the vertical direction, but have a small tilt

angle of about  $1.0^\circ$ , similar to what we observed with AFM, as mentioned above. The spacing of these reciprocal-lattice rods corresponds to a real-space periodicity of  $5.76 \text{ \AA}$ , which perfectly matches the periodicity of the  $\text{CoGe}_2(111)$  surface along its  $[11\bar{2}]$  direction, as depicted in Fig. 3 (d). Faint half-order top-facet rods can also be seen. Despite the fact that the unit mesh is actually twice as large ( $11.52 \text{ \AA}$ ) in the  $[11\bar{2}]$  direction, reflections corresponding to this periodicity (i. e., such half-order rods) are forbidden in the plane of Fig. 4 due to glide plane symmetry. (Note that the projection of the bulk-terminated real-space lattice into this plane has truly a periodicity of  $5.76 \text{ \AA}$ , as visible in Fig. 3 (d).) Hence, these faint spots might indicate a surface reconstruction or originate from multiple scattering.

The orientation of the side facets can be determined from the inclination angles of the related reciprocal-lattice rods. Two sets of such rods are particularly pronounced, with angles (relative to the  $\text{CoGe}_2(111)$  rods) of  $27.0^\circ$  (red dot-dashed lines in Fig. 4) and  $15.5^\circ$  (blue dashed lines). The respective facets' real-space periodicities as determined from the rods' spacing are  $8.09 \text{ \AA}$  and  $13.7 \text{ \AA}$ . These results can be explained by the presence of  $\text{CoGe}_2$  (113) and (112) facets, for which inclination angles and periodicities of  $27.7^\circ$  and  $16.2^\circ$ ,  $8.06 \text{ \AA}$  and  $13.4 \text{ \AA}$ , respectively, are expected, in very good agreement with experiment. The inclination angles determined with  $\mu$ -LEED are also in good agreement with the AFM data; for the type-I islands labeled "C" and "D" in Fig. 2, side facet angles between  $16^\circ$  and  $24^\circ$  are found. In case of crystallographic facets, the reciprocal facet rods intersect at bulk Bragg peak conditions [31]. Hence, from the vertical distance of these intersections, the layer spacing of the germanide islands can be determined. The experimentally obtained value of  $3.71 \text{ \AA}$  gives further support for type-I islands being of (111) orientation, since in this case an almost identical value for the layer spacing of  $3.747 \text{ \AA}$  is expected (see Fig. 3 (d)).

Having identified type-I islands as  $\text{CoGe}_2$ , and turning back to the XAS-PEEM results in Fig. 1, we can also identify type-II islands as  $\text{CoGe}_2$ , since they have virtually identical XAS fingerprints. The different morphology is probably due to a different epitaxial relationship. The latter could not be resolved in our experiments, since type-II islands are very narrow and, thus, produce only weak  $\mu$ -LEED intensity.

Regarding the peak shift of the type-I to the type-VI fingerprints towards the metallic spectrum in Fig. 1 (b), it seems reasonable to relate this peak shift to the stoichiometry of the islands, i. e., to assign an increasing peak energy to increasing Ge content, since the  $\text{CoGe}_2$  stoichiometry of type-I and type-II islands is the one with the highest Ge content (and, of course, pure Co has the lowest Ge content). Following this reasoning, type-III and type-IV islands are likely to consist of  $\text{Co}_5\text{Ge}_7$ , and type-V and type-VI islands of  $\text{CoGe}$ . Since islands of

type III and type IV are not observed on single-crystal Ge(001) substrates but only on epilayers, it is concluded that the nucleation and growth of islands with  $\text{Co}_5\text{Ge}_7$  stoichiometry is related to defects.

#### 4. Conclusion

We have shown that high-temperature reactive growth of cobalt germanide on Ge(001) leads to a variety of island morphologies, including elongated and compact structures. Moreover, a correlation of island morphology and cobalt germanide stoichiometry has been revealed by local XAS. From a detailed  $\mu$ -LEED analysis, one of the most prominent island types was identified as  $\text{CoGe}_2(111)$ , an orientation that has not been reported so far. These islands exhibit (112) and (113) side facets. In addition to  $\text{CoGe}_2$ , different germanide phases have been detected and are attributed to  $\text{Co}_5\text{Ge}_7$  and  $\text{CoGe}$ . Therefore, high-temperature reactive growth does not seem to be a superior approach to enforce single-phase cobalt germanide growth. Remarkably, the occurrence of such intermediate phases is strongly suppressed on single-crystal substrates and can thus be attributed to defects. It should be noted that this is not a general trend, since on amorphous Ge, for instance, the formation of  $\text{CoGe}_2$  has been reported without any  $\text{Co}_5\text{Ge}_7$  [32].

With respect to applications, an important conclusion is that the defect structure and defect density of Ge layers on Si play a significant role here and have to be taken into account when trying to transfer results from single-crystal based research, i. e. from the vast majority of previous literature, into device development.

#### References

- [1] Madelung O (ed) 1996 *Semiconductors — basic data* 2<sup>nd</sup> ed (Berlin: Springer Verlag)
- [2] Claeys C and Simoen E 2007 *Germanium-Based Technologies: From Materials to Devices* 1st ed (Amsterdam: Elsevier Science)
- [3] Liu J, Sun X, Pan D, Wang X, Kimerling L C, Koch T L and Michel J 2007 *Opt. Express* **15** 11272–11277
- [4] Liu J, Sun X, Camacho-Aguilera R, Kimerling L C and Michel J 2010 *Opt. Lett.* **35** 679–681
- [5] Capellini G, Reich C, Guha S, Yamamoto Y, Lisker M, Virgilio M, Ghrib A, Kurdi M E, Boucaud P, Tillack B and Schroeder T 2014 *Opt. Express* **22** 399–410
- [6] Wirths S, Geiger R, von den Driesch N, Mussler G, Stoica T, Mantl S, Ikonik Z, Luysberg M, Chiussi S, Hartmann J M, Sigg H, Faist J, Buca D and Grützmacher D 2015 *Nat. Photonics* **9** 88–92
- [7] Tung R T 2014 *Appl. Phys. Rev.* **1** 011304
- [8] Grzela T, Capellini G, Koczorowski W, Schubert M A, Czajka R, Curson N J, Heidmann I, Schmidt T, Falta J and Schroeder T 2015 *Nanotechnol.* **26** 385701
- [9] von Känel H, Schwarz C, Goncalves-Conto S, Müller E, Miglio L, Tavazza F and Malegori G 1995 *Phys. Rev. Lett.* **74**(7) 1163–1166
- [10] Vantomme A, Degroote S, Dekoster J, Langouche G and Pretorius R 1999 *Appl. Phys. Lett.* **74** 3137–3139
- [11] Ishida K and Nishizawa T 1991 *J. Phase Equilibria* **12** 77–83
- [12] Ashburn S P, Öztürk M C, Harris G and Maher D M 1993 *J. Appl. Phys.* **74** 4455–4460

- [13] Goldfarb I and Briggs G A D 2002 *J. Vac. Sci. Technol. B* **20** 1419–1426
- [14] Goldfarb I and Briggs G A D 2001 *J. Mater. Res.* **16** 744–752
- [15] Choi J, Lim D K, Kim Y and Kim S 2010 *J. Phys. Chem. C* **114** 8992–8996
- [16] Mocking T F, Hlawacek G and Zandvliet H J W 2012 *Surf. Sci.* **606** 924–927 ISSN 00396028
- [17] Grzela T, Koczorowski W, Capellini G, Czajka R, Radny M W, Curson N, Schofield S R, Schubert M A and Schroeder T 2014 *J. Appl. Phys.* **115** 074307
- [18] Sun H P, Chen Y B, Pan X Q, Chi D Z, Nath R and Foo Y L 2005 *Appl. Phys. Lett.* **86** 071904
- [19] De Keyser K, Van Meirhaeghe R L, Detavernier C, Jordan-Sweet J and Lavoie C 2010 *J. Electrochem. Soc.* **157** H395–H404
- [20] Aballe L, Foerster M, Pellegrin E, Nicolas J and Ferrer S 2015 *J. Synchrotron Rad.* **22** 745–752
- [21] Yamamoto Y, Zaumseil P, Arguirov T, Kittler M and Tillack B 2011 *Sol.-State Electron.* **60** 2–6
- [22] Johnson A D, Norris C, Frenken J W M, Derbyshire H S, MacDonald J E, Van Silfhout R G and Van Der Veen J F 1991 *Phys. Rev. B* **44** 1134–1138
- [23] Flege J I, Tang W X and Altman M S 2012 *Characterization of Materials* ed Kaufmann E N (Hoboken: John Wiley & Sons) chap Low-Energy Electron Microscopy 2nd ed
- [24] Als-Nielsen J and McMorrow D 2001 *Elements of Modern X-ray Analysis* (Hoboken: John Wiley & Sons)
- [25] Rehr J J and Albers R C 2000 *Rev. Mod. Phys.* **72** 621–654
- [26] Schubert K and Pfisterer H 1948 *Die Naturwissenschaften* **35** 222 ISSN 0028-1042, 1432-1904
- [27] Butts D A and Gale W F 2004 *Smithells metals reference book* ed Gale W F and Totemeir T C (Oxford: Elsevier Butterworth-Heinemann) chap Crystal chemistry 8th ed
- [28] Audebrand N, Ellner M and Mittemeijer E J 2000 *Powder Diffraction* **15**(2) 120–122 ISSN 1945-7413
- [29] Meyer zu Heringdorf F J and Horn-von Hoegen M 2005 *Rev. Sci. Instrum.* **76** 085102
- [30] Schmidt T, Clausen T, Flege J I, Gangopadhyay S, Locatelli A, Mentis T O, Guo F Z, Heun S and Falta J 2007 *New J. Phys.* **9** 392
- [31] Horn-von Hoegen M 1999 *Z. Krist.* **214** 591–628 and 684–721
- [32] Opsomer K, Deduytsche D, Detavernier C, Van Meirhaeghe R L, Lauwers A, Maex K and Lavoie C 2007 *Appl. Phys. Lett.* **90** 031906